Multivariate Subspace Analysis for Sensor Fusion in Subsurface Planetary Drilling Fault and Anomaly Detection

Sarah Boelter[1], Rene Mai[2], Greta Brown[1], Thomas Stucky[3], Brian Glass[4], Marybeth Wilhelm[4], Maria Gini[1]

***Abstract*— In extraterrestrial planetary environments, environmental, computing, energy, and operational constraints require robotic agents to complete tasks without human supervision. Specialized extraterrestrial robotic drilling agents like TRIDENT currently lack autonomous capabilities, primarily because research into subsurface environment representation for autonomous drilling remains in its early stages. We build upon previous field-validated work using subspace analysis methods to estimate drilling faults from drill avionics telemetry, and extend it to a multivariate subsurface anomaly detection method that leverages sensor fusion of avionics telemetry from extraterrestrial drilling robots. This method was evaluated at Mars planetary analog sites in Antarctica.**

I. Introduction

In January 2026, NASA's Space Technology Mission Directorate (STMD) identified civil space technology shortfalls requiring further development to enable future missions [1]. Among these is robotic access to subsurface environments, including autonomous deep drilling beyond current capabilities. This work focuses addressing this shortfall in the extraterrestrial robotic drill The Regolith and Ice Drill for Exploring New Terrain (TRIDENT) [2], shown in Figure 1 during field testing at Lake Untersee, a permanently ice-covered lake in Antarctica. TRIDENT is a 1-meter rotary percussive drill developed by Honeybee Robotics as a payload for NASA's 2027 VIPER mission. Autonomous extraterrestrial drilling must operate with little to no prior knowledge of the subsurface and limited ability to observe borehole conditions. Fault data is costly to obtain, as it often requires operating hardware to failure. This data scarcity limits supervised learning approaches and motivates research in model free anomaly detection methods for autonomy. In this work, we build on prior subsurface anomaly detection technique, Enhanced Singular Spectrum Transformation (ESST) [3], and extend it into the multivariate. The contributions are:

- An extended method for multivariate fault and anomaly detection, Multivariate Enhanced Singular Spectrum Transformation (MESST), which fuses avionics telemetry from multiple TRIDENT sensors. MESST provides signal stability and denoising in environments requiring autonomy.
- An evaluation of MESST in a planetary analog in Antarctica.

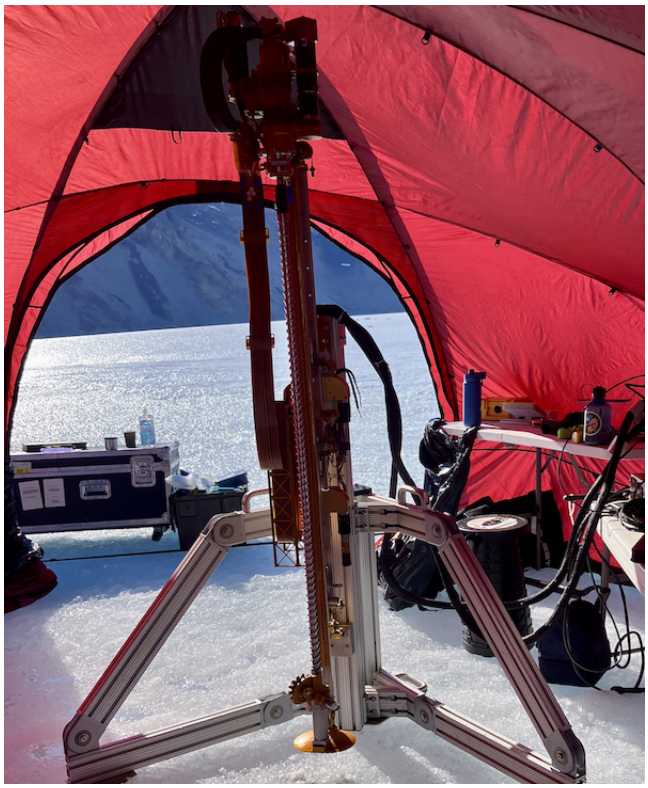


Fig. 1. Drill at Lake Untersee for field testing in Antarctica January 2026

II. Related Work

A. Subsurface Exploration in Planetary Environments

Operation and autonomy in extraterrestrial subsurface environments remains challenging. The heavy Soviet Luna 16, 20, and 24 landers of the 1970s could drill up to 2 meters due to their mass, unlike modern ∼200 kg rovers [4]. This has driven research into lightweight drilling systems [5], [2]. Other planetary subsurface exploration efforts include burrowing robots [6], the Lunar Leaper [7] legged robot for exploring the lunar subsurface, Scarab lunar rover equipped with a NORCAT drill [8], and the Exobiology Extant Life Surveyor (EELS), a snake-like robot for exploring vents on Saturn's moons [9].

B. Timeseries Subspace Tracking

Subspace tracking is a technique that maintains a continuously updated low-dimensional representation of stream-

*This work is supported by NASA Drilling in GIFT

[1]University of Minnesota Twin-Cities, Minneapolis, Minnesota 55416, USA {boelt072, brow6802, gini}@umn.edu

[2]University of Michigan, Ann Arbor, Michigan, 48109, USA {renemai}@umich.edu

[3]KBR Wyle Services LLC, Moffett Field, California 94043, USA {thomas.stucky}@nasa.gov

[4]NASA Ames Research Center, Moffett Field, California 94043, USA {brian.glass, marybeth.wilhelm}@nasa.gov

ing data, enabling detection of changes in the underlying signal or system behavior. These methods are well-suited for noisy or incomplete data and for settings with limited computational resources [10]. Common approaches include GROUSE [11] and PETRELS [12], where PETRELS generally provides faster and more robust convergence at the cost of increased computational complexity.

Subspace-based change-point detection (CPD) methods detect abrupt morphological changes without relying on long historical sequences. They focus on signal structure rather than statistical properties and suppress noise through subspace decomposition. While this reduces compatibility with statistical CPD methods [13] and limits long-term temporal context, these methods remain effective for detecting sudden changes. Subspace-based CPD typically uses singular value decomposition (SVD) of trajectory matrices to extract representative subspaces before and after a time t, comparing them to produce a change-point score [14], [15]. A widely used formulation is Singular Spectrum Transformation (SST) [14], [16], which measures change by contrasting subspace features across time windows.

C. Sensor Fusion in Signal Processing and Robotics

Sensor fusion combines data from multiple sensors to improve estimation of a system's state. The choice of methods depends on the number of sensors, data volume, and available computational resources, which strongly affect performance. Applications span industrial systems such as power plants [17], in-process defect detection in welding [18], and robot localization [19], as well as denoising and feature extraction across heterogeneous sensor streams [20].

Many sensing problems exhibit low-dimensional structure, enabling efficient storage and computation. SVD and proper orthogonal decomposition (POD) extract dominant spatial modes but do not explicitly model temporal dynamics. Hankel matrices formed from time-delayed embeddings, where each column represents a temporal window, scale linearly with space, time, and embedding dimension, and their SVD provides a discrete approximation of space-time POD [21]. Hankel-based methods are widely used in applications such as seismic denoising [22], bearing and spindle fault detection [23], structural system identification [24], and rotating machinery fault diagnosis [25].

III. Methods

A. Multivariate ESST

This section presents MESST. We review the role of Hankel matrices in univariate and multivariate time-series processing and summarize ESST, which has shown strong performance in univariate drill telemetry fault and anomaly detection. MESST extends ESST to the multivariate case using a block Hankel matrix, enabling sensor fusion that reduces change score noise and produces clearer and more reliable fault and anomaly signals than a single stream alone.

1) Block Hankel: Hankel matrices applied to time-series data contain the time history of data, with ascending skew-diagonal entries identical [21]. Hankel matrices have been used successfully with change point detection for monitoring singular timeseries drilling telemetry [3]. Suppose a sensor produces a univariate stream of timeseries measurements $a(t)$, such that the stream of measurements is $a(t) = \begin{bmatrix} a(1) & a(2) & \dots & a(\delta t + p - 1) \end{bmatrix}^T$. Here, δt is the number of time regressions stored in the Hankel matrix's columns, and p is the length of data stored in the matrix's rows; traditionally, $\delta t = p$, yielding a symmetric Hankel matrix. The resulting univariate Hankel matrix formed from this sensor is

$$\mathbf{H}(a(t)) = \begin{bmatrix} a(t) & a(t-1) & \dots & a(t-\delta t) \\ a(t-1) & a(t-2) & \dots & a(t-\delta t-1) \\ \vdots & \vdots & \ddots & \vdots \\ a(t-p) & a(t–p–1) & \dots & a(t–\delta t–p–1) \end{bmatrix}, \quad (1)$$

where t represents the time at which the matrix was formed and $t \geq \delta t + p + 1$ to avoid zero entries in the Hankel matrix. This Hankel matrix is univariate and can be used for various applications [22], [23], [24], [25].

If multiple sensors provide separate univariate time-series measurements relating to a monitored process, it may be advantageous to combine the separate univariate timeseries measurements into a multivariate Hankel matrix. Let timeseries multivariate vector $\vec{q}(t)$ represent the measurements from k sensors at time t, such that $\vec{q}(t) = \begin{bmatrix} q_1(t) & q_2(t) & \dots & q_k(t) \end{bmatrix}$. A block Hankel matrix $\mathbf{H}(\vec{q}(t))$ can formed from the entries of $\vec{q}(t)$ as

$$\mathbf{H}(\vec{q}(t)) = \begin{bmatrix} \vec{q}(t) & \vec{q}(t-1) & \dots & \vec{q}(t-\delta t) \\ \vec{q}(t-1) & \vec{q}(t-2) & \dots & \vec{q}(t-\delta t-1) \\ \vdots & \vdots & \ddots & \vdots \\ \vec{q}(t-p) & \vec{q}(t–p–1) & \dots & \vec{q}(t–\delta t–p–1) \end{bmatrix}. \quad (2)$$

Using the block Hankel matrix instead of the univariate matrix allows the use of techniques leveraging the relationship between different related sensors.

2) ESST: Subspace-based CPD methods have been used with drill avionics data in the past because they are uniquely suited for detecting sudden changes without requiring training. These methods do not extract statistical properties and ignore noise, as the decomposition acts as a filter for random signal contributions. Subspace-based CPD methods use the singular value decomposition of of two Hankel matrices $\mathbf{H}_i$ and $\mathbf{H}_j$ with $i < t < j$ to extract representative sequences before and after ($\pm\delta t$) some point in time t and compare them to provide a change point score [14], [15]. In the past, ESST outperformed SST and other methods for the noisy signals encountered for robotic drills [3].

ESST embeds both past and future subsequences into a single matrix and extracts the score by analyzing whether there are major characteristics that are only present in either past or future subsequences. With that, we can incorporate more information from the future subsequences into our final change score. We analyze the k-major right singular vectors

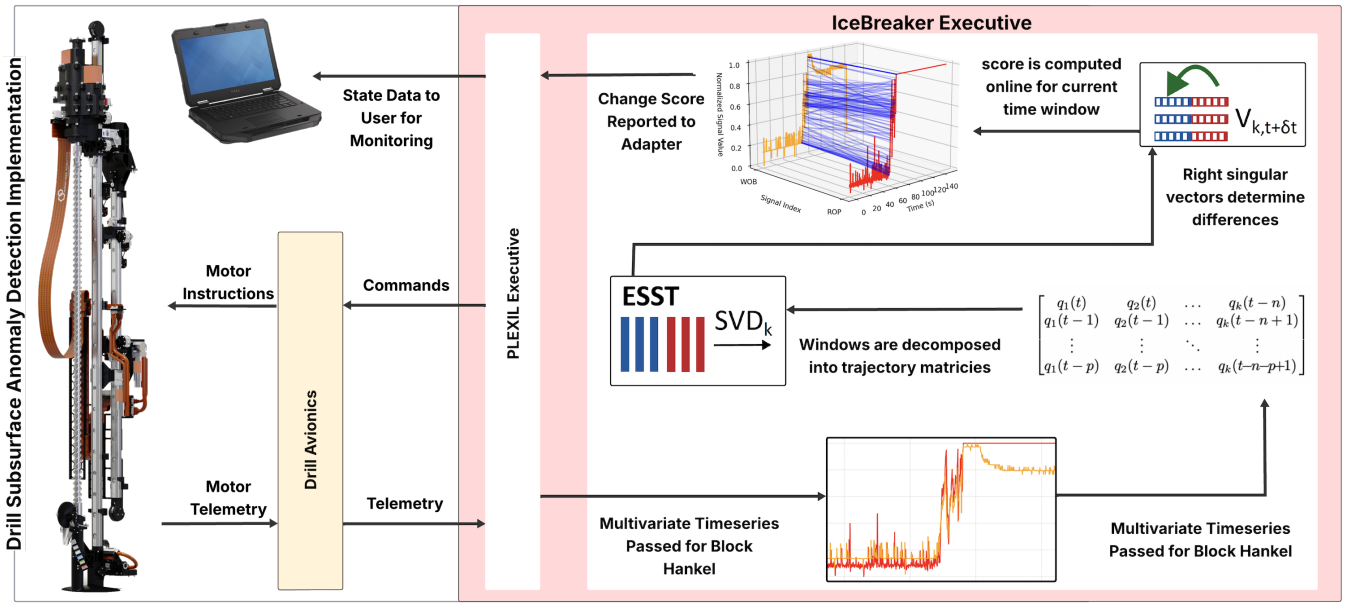


Fig. 2. Multivariate Subsurface Anomaly Detection Implementation. Motor Telemetry comes into the drill avionics. It is fed to the PLEXIL executive at a rate of 40Hz, and passes windows of data to our MESST Module. The data windows are then decomposed into block Hankel matrices, and the right singular vectors determine any significant changes, which are then used to compute the multivariate score. The change score is then passed to the user.

$\mathbf{V}_k$ of our two-sided Hankel matrix, where the first half of the columns are time series subsequences from time t, and the second half are time series subsequences around time $t + \delta t$:

$$\tilde{S}_T^t = \frac{\sum_{i=0}^{k-1} \sigma_i \left| \frac{1}{N} \left(\sum_{j=0}^{n/2-1} \mathbf{V}^{i,j} - \sum_{j=n/2}^{n-1} \mathbf{V}^{i,j} \right) \right|}{\sum_{i=0}^{k-1} \sigma_i}. \quad (3)$$

Using more characteristics yields a more complete representation of the time series. Accordingly, the improved change score is computed from multiple vectors of both Hankel matrices. The ESST algorithm enables this by modifying the Hankel matrix construction and utilizing the previously unused right singular vectors $\mathbf{V}_{t,k}$. The ESST method parameters include rank k of the subspace, the number of sequences n, and the length w of the subsequences that make up the Hankel matrices, which are δt apart. For the Antarctic field exercise, we fixed $\delta t = w/3$ to a third of the window size. From previous work, we found $k = 5$ and $w = 70$ works for accurate online fault and anomaly detection with a telemetry sample rate of $f_s = 40$ Hz.

3) MESST: In univariate ESST, we analyze the k-major right singular vectors V_k of our two-sided Hankel matrix, where the first half of the columns are time series subsequences from time t, and the second half are time series subsequences around time $t + \delta t$. Using ESST with multiple timeseries, to obtain the benefit of sensor fusion, requires formulating the multivariate block Hankel matrix [21]. Other techniques can be applied to the block Hankel matrix as normal. We construct a two-sided block Hankel matrix by taking $\mathbf{H}(\vec{q}(i))$ and $\mathbf{H}(\vec{q}(j))$ where $i < t < j$

$$\mathbf{H}_{ij} = [\mathbf{H}(\vec{q}(i)) \mid \mathbf{H}(\vec{q}(j))]. \quad (4)$$

This embeds both past and future multivariate subsequences into a single matrix. The first block contains subsequences centered at time t, while the second block contains subsequences centered at $t + \delta t$. We then take the SVD

$$\mathbf{H}_{ij} = \mathbf{U}\mathbf{\Sigma}\mathbf{V}^{i,j}. \quad (5)$$

We take $\mathbf{V}^{i,j}$ and incorporate it into (3). This allows us to analyze the k-dominant right singular vectors $\mathbf{V}_k$ to obtain a change score that captures and enhances the multivariate differences between past and future subsequences into the final score while minimizing noise.

B. Methods of Evaluation

Evaluation of CPD and subspace distance metric algorithms remains highly application-dependent, and while benchmarks [26] provide comparative frameworks, they may not fully capture the characteristics of noisy real-world sensor data. We selected and evaluated methods based on the specific constraints of our application.

1) Change Score Variance: A primary motivation for sensor fusion is reducing noise while enhancing fault-related signal characteristics. Although ESST has demonstrated effective fault detection on drill telemetry, the resulting change-score signals can themselves be noisy.

We evaluate signal noise using variance [27]:

$$\sigma^2_{score} = \frac{1}{n} \sum_{i=1}^{n} (x_i - \mu)^2 \quad (6)$$

Computing variance over an entire change-score signal is not useful because fault events intentionally produce large changes in the mean. Instead, we evaluate nominal and faulty segments separately. Let (a) denote the start of drilling, (b)

the fault onset, and (c) the end of the fault. The variance of a nominal segment is

$$\sigma^2_{[a,b]} = \frac{1}{b-a+1} \sum_{t=a}^{b} \left(x_t - \mu_{[a,b]}\right)^2 \tag{7}$$

where $\mu_{[a,b]}$ is segment mean ([a,b]). We define the nominal and faulty variances as $\sigma_n = \sigma^2_{[a,b]}$ and $\sigma_f = \sigma^2_{[b,c]}$, respectively, with the objective to minimize σ_n while maximizing σ_f, for reduced noise during nominal operation and stronger fault signals during anomalies.

2) Visual: In the time series anomaly detection field, there has been valid criticism of the evaluation benchmarks of many approaches [28]. To mitigate the effects of potentially mislabeled or misleading results due to the compression of the results into scalar metrics, we provide some visual results for qualitative analysis.

IV. Problem Formulation

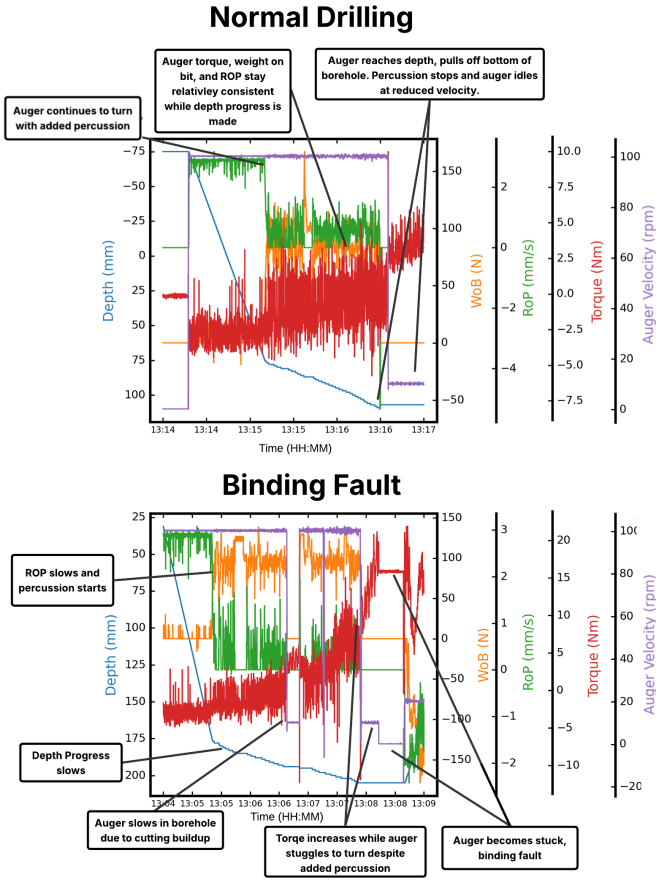


Fig. 3. Time-series data showing Depth, Weight on Bit, Rate of Penetration, Auger Velocity, and Auger Torque during incremental drilling. The top image shows normal drilling. The bottom image shows a binding fault, where Torque and Weight on Bit spike, Auger Velocity decreases, and the auger becomes stuck in the borehole.

Figure 3 shows time-series from two boreholes, one representing normal drilling and the other a fault condition. In general, faults are characterized by increases in motor torque τ and weight on bit ϕ, while the rate of penetration ρ drops toward zero. The auger velocity ω often exhibits sudden dips due increased friction preceding a fault [3]. We formulate this as an online change point detection (CPD) problem where telemetry is streamed at $f_s = 40$ Hz and represented as:

$$\mathbf{x}(t) = \begin{bmatrix} x^{(\tau)}(t) \\ x^{(\phi)}(t) \\ x^{(\rho)}(t) \\ x^{(\omega)}(t) \end{bmatrix} \in \mathbb{R}^4, \qquad \mathcal{P} = \{(\tau,\omega),(\phi,\rho)\}, \tag{8}$$

where $x^{(\tau)}(t)$ denotes motor torque, $x^{(\phi)}(t)$ weight on bit (WoB), $x^{(\rho)}(t)$ rate of penetration (ROP), and $x^{(\omega)}(t)$ auger velocity. The set $\mathcal{P}$ defines the sensor fusion pairs for MESST. Each channel is normalized online using a sliding-window buffer

$$\tilde{x}^{(c)}(t) = \frac{x^{(c)}(t) - \mu_B^{(c)}}{\sigma_B^{(c)} + \epsilon}, \quad c \in \{\tau,\phi,\rho,\omega\}. \tag{9}$$

Rather than analyzing channels independently, MESST jointly embeds each sensor pair into a block Hankel matrix. For a pair $(a,b) \in \mathcal{P}$, the block Hankel matrix is defined as

$$\mathbf{H}_{t,(a,b)} = \left[\mathbf{H}_{t,(a)} \;\middle|\; \mathbf{H}_{t,(b)}\right], \tag{10}$$

which embeds the joint temporal structure of both signals into a shared subspace. As illustrated in Figure 4, faulty telemetry often manifests simultaneously across channel pairs with differing magnitudes and dynamics. Combining signal pairs into a block Hankel matrix allows MESST to capture correlated structural changes directly in the decomposition, improving denoising. The block Hankel matrix is decomposed via truncated SVD. The MESST change score $S_t^{(a,b)}$ is computed using the right singular vectors as defined in Eq. (3). This formulation yields a set of MESST score streams for denoised change scores.

V. Experiments

Our experimental setup follows [3] with modifications for block Hankel multivariate time-series monitoring. As shown in Figure 2, drill avionics provide multiple telemetry streams to the PLEXIL Executive, which forwards incremental multivariate data to the MESST module. Past and current block Hankel matrices are constructed from each time window, concatenated, and analyzed using right singular vectors to compute a change score that is presented to the operator.

A. Planetary Analog MESST Validation

1) Field Site Evaluation and Testing Protocol: In January 2026, an interdisciplinary team conducted drilling tests at several sites in Queen Maud Land, Antarctica, selected for their cold-desert, ice-free Mars-analog characteristics [29], [30], including shallow permafrost and relevant geomorphic processes. Additional testing was performed on the stable ice cover of Lake Untersee. Because prior work already validated ESST for fault detection in field drilling operations, our focus is not fault-detection performance but the effectiveness of MESST sensor fusion for noise reduction and

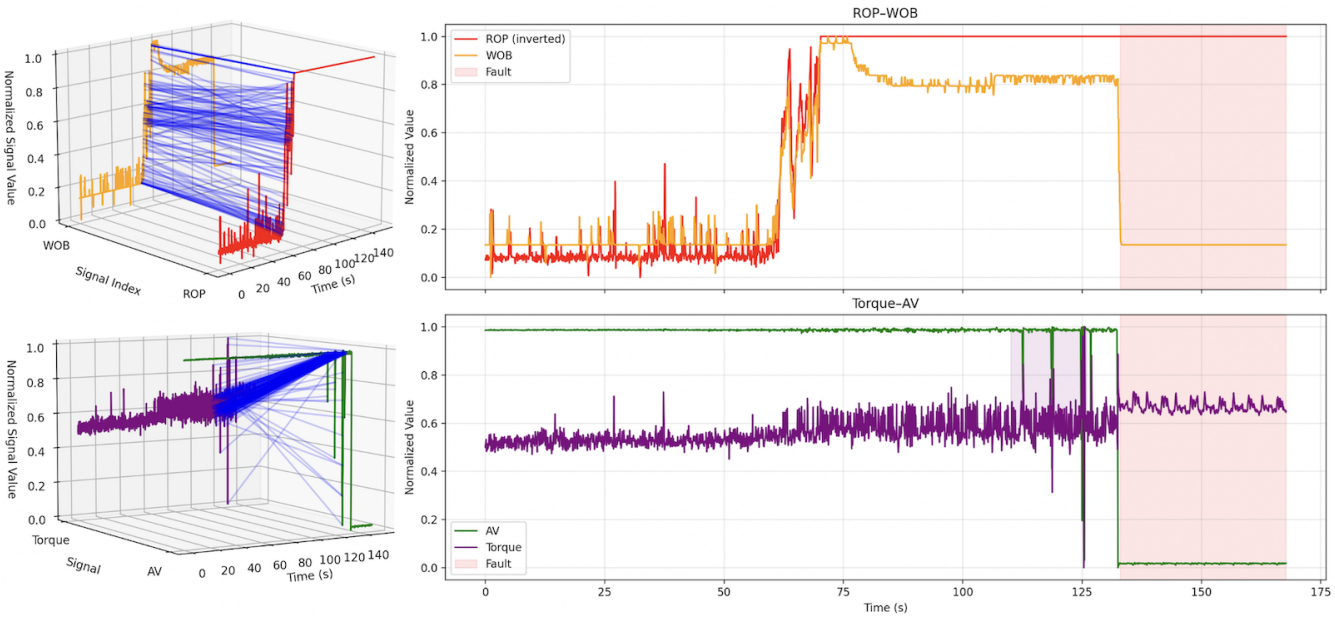


Fig. 4. Top graph is inverted rate of penetration ϕ and weight on bit ρ telemetry streams. Bottom graph is torque τ and auger velocity ω telemetry streams. The left graphs illustrate how similar changes in complimentary telemetry could be used for sensor fusion.

signal enhancement. In Figure 5e compare univariate ESST scores with multivariate MESST scores generated from fused telemetry signals. Specifically, torque (S_τ) and auger velocity (S_ω) are fused to produce $S_{\tau,\omega}$, while rate of penetration (S_ρ) and weight on bit (S_ϕ) are fused to produce $S_{\rho,\phi}$.

For evaluation, score signals are divided into nominal (σ_n) and faulty (σ_f) regions as defined in Sec. III-B.1. We seek to minimize variance in nominal regions and maximize variance in faulty regions using Equation 7. Because fused signals often combine measurements with similar trends but different noise characteristics (see Figure 4), we do not necessarily expect lower nominal variance than both source signals. Instead, successful fusion should reduce variance relative to at least the noisier input while ideally increasing variance during faults relative to at least one input. The most favorable outcome would be lower variance than both source signals in nominal regions and higher variance than both during faults.

Overall, we evaluate whether sensor fusion produces more robust change scores by suppressing nominal noise and enhancing fault-related deviations, thereby improving qualitative and quantitative fault detection.

VI. Results

During field testing, we monitored telemetry variables τ, ρ, ϕ, and ω and and their respective change scores S_τ, S_ϕ, S_ρ, S_ω, along with multivariate sensor fusion scores $S_{\tau,\omega}$ and $S_{\rho,\phi}$.

A. Planetary Analog MESST Field Validation

We encountered nine instances of faults in our Antarctic Field test drilling. We did not evaluate three because of software bugs. In the remaining faults, we evaluated the variance of the univariate ESST scores and multivariate MESST sensor fusion scores over the σ_n and σ_f segments, and the weighted averages of these variances were taken across our samples. We processed and evaluated signals first visually and against field notes and log files with timestamps, similar to in Figure 3. This is so we could best judge fault symptom onset, and mark timestamps before evaluating both ESST and MESST change scores.

TABLE I

Weighted average variance for nominal (σ_n) and faulty (σ_f) segments

Signal	$\sigma^2(\sigma_n)$	$\sigma^2(\sigma_f)$
$S_{\tau,\omega}$	0.001378	0.082164
S_τ	0.006287	0.046934
S_ω	0.000000	0.024155
$S_{\rho,\phi}$	0.026078	0.050281
S_ρ	0.027251	0.065119
S_ϕ	0.019044	0.025253

The first sensor fusion grouping evaluation $S_{\tau,\omega}$, S_τ, and S_ω is in Table I. From the numerical observations, for σ_n, the sensor fusion helped significantly reduce the noise in S_τ, while slightly increasing the variance from S_ω. For our σ_f, the variance of our $S_{\tau,\omega}$ increased significantly over the individual S_τ and S_ω signals, which means the sensor fusion significantly increased the faulty section variance. For the second sensor fusion grouping evaluation $S_{\rho,\phi}$, S_ρ, and S_ϕ, both signals had some noise in the σ_n grouping, with S_ρ being significantly more noisy than S_ϕ. However, the overall $S_{\rho,\phi}$ did decrease compared to the most noisy signal. For our σ_f, the variance of our $S_{\rho,\phi}$ increased over the individual S_ϕ signals, which means the sensor fusion increased the faulty section variance for one of the signals.

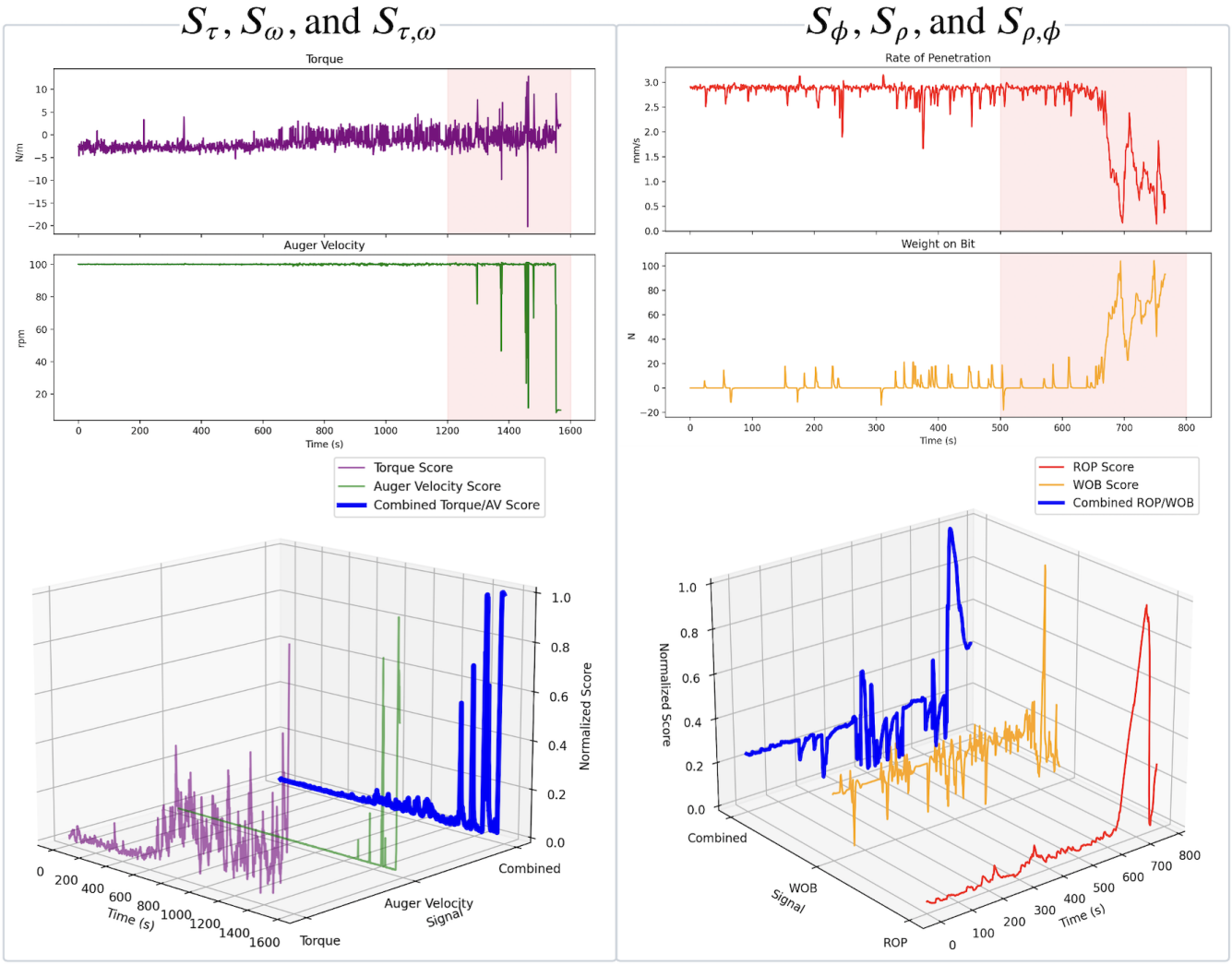


Fig. 5. Left set of graphs shows torque τ, auger velocity ω signals and right set of graphs shows rate of penetration ρ and weight on bit ϕ. Bottom set of graphs show respective individual ESST change scores and fused MESST scores for respective telemetry signals.

VII. Discussion

For $S_{\tau,\omega}$, comparison of the variance analysis with the signal plots indicates that MESST was successful. The fused signal $S_{\tau,\omega}$ significantly reduced noise in S_τ for our σ_n segments. Although variance increased slightly in S_ω, the baseline noise level in this signal is extremely low (on the order of 10^{-8})–(10^{-9}), making the increase visually negligible (Figure 5). For our σ_f segment, variance generally increased in $S_{\tau,\omega}$ relative to both S_τ and S_ω, representing the desired outcome. Similarly, for $S_{\rho,\phi}$, the fused signal reduced noise in S_ρ for our σ_n segments, while variance increased relative to S_ϕ during the σ_f segment.

Fault-onset detection time is critical for mitigation. Prior results show ESST's small lag still provides sufficient lead time, and we wanted to ensure MESST did not introduce detection lag. Despite limited field hardware, score computation kept pace with drilling operations, with no meaningful runtime difference between ESST and MESST, confirming practical efficiency.

Field operations included hardware failures (drill and primary computer malfunctions requiring on-site repair) and software issues requiring updates via Starlink. This highlights the realities of field robotics and the importance of redundancy and preparation. Overall, MESST performed successfully on real-world field datasets. Quantitatively and qualitatively, it reduced noise in $S_{\tau,\omega}$ and improved fault-detection performance, while also reducing noise in $S_{\rho,\phi}$ without degrading reliability. Given the minimal increase in computational cost, these results are encouraging.

VIII. Conclusions and Future Work

This work presented a method for multivariate fault and anomaly detection, MESST, and a field evaluation of MESST in Antarctica. We found MESST enhanced effectiveness for identifying faults and anomalies, allowing better fault identification and detection using sensor fusion. Future work involves incorporating these fault and anomaly detection methods into autonomous drilling.

REFERENCES

[1] N. S.T.M.D., "2026 civil space shortfalls," 2026. [Online]. Available: https://www.nasa.gov/wp-content/uploads/2026/03/2026-civil-space-shortfalls.pdf?emrc=7ef4d2

[2] K. Zacny, P. Chu, V. Vendiola, P. Creekmore, P. Ng, S. Goldman, E. Seto, K. Bywaters, E. Bailey, R. Zheng, I. King, A. Rashedi, P. Chow, R. Huddleston, G. Paulsen, A. Wang, J. Wilson, J. Quinn, A. Eichenbaum, J. Captain, J. Kleinhenz, E. Rezich, D. Lim, Z. Mirmalek, D. Lees, R. Elphic, K. E. Smith, T. Colaprete, V. Bickel, K. Lewis, and T. Viper Teams, Prime-1, "Development of TRIDENT Drill for Ice Mining on the Moon with NASA PRIME-1 and VIPER Missions," in *Earth and Space 2024*. Miami, Florida: American Society of Civil Engineers, Oct. 2024, pp. 280–293. [Online]. Available: https://ascelibrary.org/doi/10.1061/9780784485736.026

[3] S. Boelter, G. Brown, L. Weber, T. Stucky, B. Glass, and M. Gini, "Model-free subsurface anomaly detection using subspace analysis techniques for sparse telemetry for extraterrestrial drilling robots," *Proc. IEEE Int'l Conf. on Robotics and Automation (ICRA), in press*, 2026.

[4] G. Paulsen, K. Zacny, P. Chu, E. Mumm, K. Davis, S. Frader-Thompson, K. Petrich, D. Glaser, P. Bartlett, H. Cannon, and B. Glass, *Robotic Drill Systems for Planetary Exploration*. AIAA, 2006.

[5] B. Glass, A. Wang, S. Huffman1, K. Zacny, and P. Lee1, "Lita drill tests at haughton crater," *45th Lunar and Planetary Science Conference 2014*, 2014.

[6] Y. Liu, Z. Yuan, Y. Li, and H. Zhao, "A Three-dimensional path planning method of autonomous burrowing robot for lunar subsurface exploration," in *2021 6th IEEE International Conference on Advanced Robotics and Mechatronics (ICARM)*, Jul. 2021, pp. 710–715. [Online]. Available: https://ieeexplore.ieee.org/document/9536059/

[7] H. Kolvenbach *et al.*, "Lunarleaper—a mission concept to explore the lunar subsurface with a small-scale legged robot," *Acta Astronautica*, vol. 240, pp. 63–75, 2026. [Online]. Available: https://www.sciencedirect.com/science/article/pii/S0094576525008082

[8] P. W. Bartlett, D. Wettergreen, and W. R. L. Whittaker, "Design of the scarab rover for mobility and drilling in the lunar cold traps," in *Proceedings of the International Symposium on Artificial Intelligence, Robotics and Automation in Space (i-SAIRAS '08)*, 2008, pp. 3–6.

[9] T. S. Vaquero *et al.*, "EELS: Autonomous snake-like robot with task and motion planning capabilities for ice world exploration," *Science Robotics*, vol. 9, no. 88, p. eadh8332, Mar. 2024. [Online]. Available: https://www.science.org/doi/full/10.1126/scirobotics.adh8332

[10] L. Balzano, Y. Chi, and Y. Lu, "Streaming PCA and subspace tracking: The missing data case," *Proceedings of the IEEE*, vol. PP, 2018.

[11] L. Balzano, R. Nowak, and B. Recht, "Online identification and tracking of subspaces from highly incomplete information," in *2010 48th Annual Allerton Conference on Communication, Control, and Computing (Allerton)*, 2010, pp. 704–711.

[12] Y. Chi, Y. C. Eldar, and R. Calderbank, "PETRELS: Parallel subspace estimation and tracking by recursive least squares from partial observations," *IEEE Transactions on Signal Processing*, vol. 61, no. 23, pp. 5947–5959, 2013.

[13] S. Liu, M. Yamada, N. Collier, and M. Sugiyama, "Change-point detection in time-series data by relative density-ratio estimation," *Neural Networks*, vol. 43, 2013.

[14] T. Idé and K. Tsuda, "Change-point detection using Krylov subspace learning," in *Proceedings of the SIAM International Conference on Data Mining*, 2007, pp. 515–520.

[15] V. Moskvina and A. Zhigljavsky, "An algorithm based on singular spectrum analysis for change-point detection," *Communications in Statistics-Simulation and Computation*, vol. 32, no. 2, 2003.

[16] L. Weber and R. Lenz, "Accelerating singular spectrum transformation for scalable change point detection," *IEEE Access*, vol. 13, pp. 213 556–213 577, 2025.

[17] ——, "Machine learning in sensor identification for industrial systems," *it - Information Technology*, vol. 65, pp. 213 556–213 577, 2023.

[18] F. Deng, Y. Huang, S. Lu, Y. Chen, J. Chen, H. Feng, J. Zhang, Y. Yang, J. Hu, T. L. Lam, and F. Xia, "A multi-sensor data fusion system for laser welding process monitoring," *IEEE Access*, vol. 8, pp. 147 349–147 357, 2020.

[19] Z. Huang, G. Ye, P. Yang, and W. Yu, "Application of multi-sensor fusion localization algorithm based on recurrent neural networks," *Scientific Reports*, vol. 15, no. 1, p. 8195, 2025. [Online]. Available: https://doi.org/10.1038/s41598-025-90492-4

[20] S. Yao, S. Hu, Y. Zhao, A. Zhang, and T. Abdelzaher, "Deepsense: A unified deep learning framework for time-series mobile sensing data processing," in *Proc. 26th Int'l Conference on World Wide Web*, ser. WWW '17. Geneva, CH: International World Wide Web Conferences Steering Committee, 2017, p. 351–360. [Online]. Available: https://doi.org/10.1145/3038912.3052577

[21] P. Frame and A. Towne, "Space-time POD and the Hankel matrix," *PLOS ONE*, vol. 18, no. 8, pp. 1–31, 08 2023. [Online]. Available: https://doi.org/10.1371/journal.pone.0289637

[22] D. Zhang, J. He, Y. Zhou, D. Chen, and Z. Wang, "Hybrid low-rank and sparsity constraint with hankel structure preservation for simultaneous seismic reconstruction and denoising," *IEEE Geoscience and Remote Sensing Letters*, vol. 20, pp. 1–5, 2023.

[23] W. Sun, Y. Zhou, J. Xiang, B. Chen, and W. Feng, "Hankel matrix-based condition monitoring of rolling element bearings: An enhanced framework for time-series analysis," *IEEE Transactions on Instrumentation and Measurement*, vol. 70, pp. 1–10, 2021.

[24] F. Golnary, H. Kalhori, B. Li, and B. Halkon, "Hankel matrix denoising for enhanced subspace state–space system identification in modal analysis," *Mechanical Systems and Signal Processing*, vol. 246, p. 113843, 2026. [Online]. Available: https://www.sciencedirect.com/science/article/pii/S0888327025015444

[25] Y. Zhang, M. Yu, Y. Wang, and C. Han, "A rubbing fault identification method of combining the covariance of the Hankel matrix and 1D-LBP," *Structural Health Monitoring*, vol. 0, no. 0, p. 14759217251340663, 2025. [Online]. Available: https://doi.org/10.1177/14759217251340663

[26] G. J. J. van den Burg and C. K. I. Williams, "An evaluation of change point detection algorithms," arXiv:2003.06222v3 [stat.ML], 2020.

[27] M. Basseville and I. Nikiforov, *Detection of Abrupt Change Theory and Application*, 04 1993, vol. 15.

[28] R. Wu and E. J. Keogh, "Current time series anomaly detection benchmarks are flawed and are creating the illusion of progress," *IEEE Transactions on Knowledge and Data Engineering*, vol. 35, no. 3, pp. 2421–2429, 2021.

[29] R. Hoover, "Schirmacher oasis/lake untersee antarctica astrobiology expedition expedition report flag 162," United States Space and Rocket Center, Tech. Rep., 05 2008.

[30] C. P. McKay, D. Andersen, and A. Davila, "Antarctic environments as models of planetary habitats: University Valley as a model for modern Mars and Lake Untersee as a model for Enceladus and ancient Mars," *The Polar Journal*, vol. 7, no. 2, pp. 303–318, 2017. [Online]. Available: https://doi.org/10.1080/2154896X.2017.1383705